Gas-Particle Flow in a Vertical Pipe with Particle-Particle Interactions

A theory is presented for the fully-developed flow of gas and particles in a vertical pipe. The relation between gas pressure gradient and the flow rates of the two phases is predicted, over the whole range of cocurrent and countercurrent flows, together with velocity profiles for both phases and the radial concentration profile for the particles. The gas and the particles interact through a drag force depending on their relative velocity, and there are mutual interactions between pairs of particles through inelastic collisions. This model is shown to account for marked segregation of gas and particles in the radial direction, and the predicted relation between the pressure gradient and the flow rates of the two phases is surprisingly complex.

J. L. Sinclair
R. Jackson
Princeton University
Princeton, NJ 08544

Introduction

Particulate solids can be transported through pipes by the action of a flowing fluid, which may be liquid or gas. The direction of flow may be vertically upward, as in risers, vertically downward, as in standpipes (which are capable of moving particulate material from regions of lower to regions of higher gas pressure), or through ducts of any intermediate inclination. When the axis of the pipe is not vertical, it is clear that the particles will be distributed nonuniformly over the cross section as a result of gravitational sedimentation; therefore, one-dimensional theoretical treatments are inappropriate. However, experimental studies of the cross-sectional distribution of particles in vertical flow (Bartholomew and Casagrande, 1957; Saxton and Worley, 1970; Yerushalmi et al., 1978; Youchou and Kwauk, 1980; Weinstein et al., 1984) reveal that, here also, there is marked segregation of the particles over the cross section. In some cases, they are found to be concentrated near the pipe wall, while in others, large regions of high concentration, called streamers, extend well into the center of the pipe. As a consequence, one-dimensional theoretical models have been unsuccessful in making quantitative predictions without the injection of a good deal of empiricism in the form of fitted parameter values which are, unfortunately, dependent on the nature of the particles and the size of the pipe.

Perhaps more seriously, there appear to be qualitative features of the overall behavior that are not adequately represented; for example, the existence of more than one regime for cocurrent downflow of particles and gas at specified flow rates under certain circumstances. Among one-dimensional models of flow in risers we mention those of Hinze (1962), Gidaspow and Solbrig (1976), Arastoopour et al. (1982), and Arastoopour and Cutchen (1985). Models for standpipe flow, which allow also for the possibility of sliding packed beds of particles in the pipe, have been presented by Leung and Jones (1978), Ginestra et al. (1980), and Chen et al. (1984).

The primary, large-scale effect of lateral segregation over the cross section is to generate cross-sectional average values of the slip velocity between particles and gas, which greatly exceed the local slip anywhere in the pipe. This results from relative motion between regions of high and low particle concentrations, and cannot be predicted without some way of predicting the distribution of particle concentration over the cross section. The central problem in constructing a more satisfactory model for pneumatic transport systems is, therefore, to understand and quantitatively model the mechanism that gives rise to the observed lateral segregation.

In most cases of interest in pneumatic transport, the Reynolds number for the gas flow, based on the pipe diameter, is high and the flow is, therefore, expected to be turbulent, at least at low particle concentrations. The effect of turbulent eddies is to disperse suspended particles that are small enough to follow the turbulent motion of the gas. For larger particles whose inertia is significant, however, it is possible that the motion induced by interaction with the eddies could lead to an uneven distribution of particles over the cross section. This view has been adopted recently by Berker and Tulig (1986), but its consequences are difficult to develop without heavy reliance on empiricism, because the effect of the particles on the structure of the turbulence is not known. Indeed, it is not easy to define what is meant in speaking of turbulent motion of the gas. In an empty pipe,

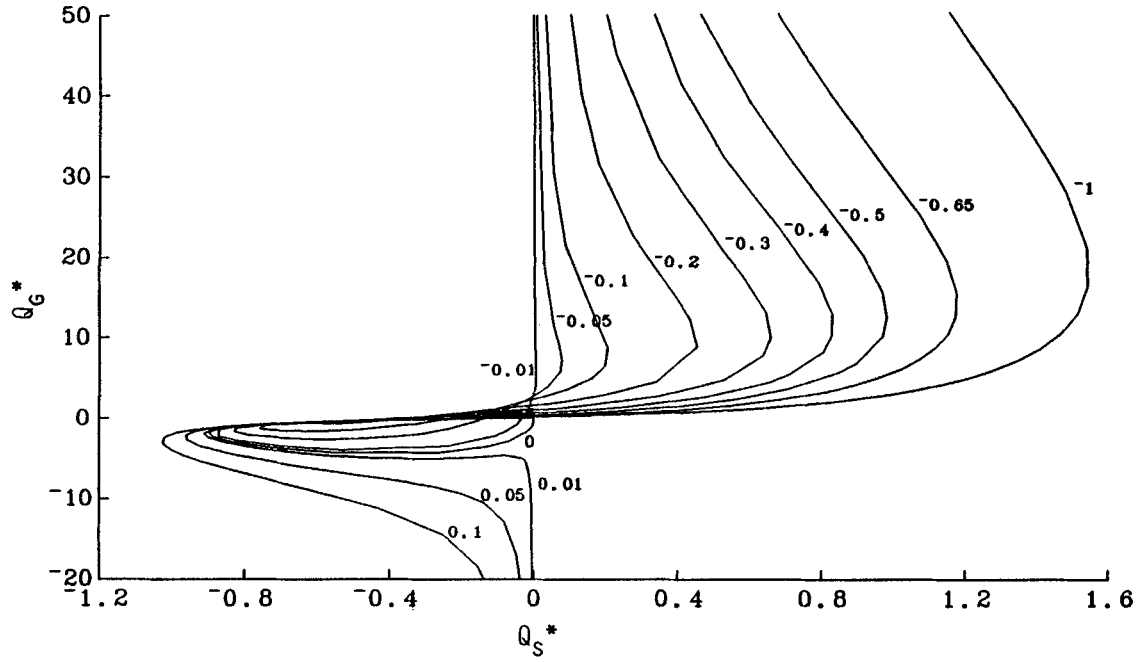

Figure 1. Contours of dp^*/dz^* in the (Q_s^*, Q_g^*) plane.

turbulence is the fluctuating component of the gas velocity induced by the shear field over the section of the pipe. When particles are present there will also be fluctuations of the gas velocity induced by the fluctuations in velocity of the particles and, on the smaller scale of a single particle, the gas flow in the boundary layer round the particle may be either laminar or turbulent.

In the motion of a gaseous suspension, both the fluid and particle velocities have local average and random components, and a realistic picture of the mechanical behavior of such a system must include a variety of interactions that depend on the two velocity fields.

1. Interaction between particles and gas that results from the difference between their mean velocity fields, and gives rise to the drag force that propels the nonrandom part of the particle motion.

2. Interaction of the particles with the fluctuating component of the gas velocity. This may cause a flux of kinetic energy in either direction between the fluctuating components of velocity of the two phases, either damping the fluctuations of gas velocity and stimulating fluctuations in particle velocity, or vice versa.

3. Interactions of the fluctuating part of the particle motion with the mean particle motion through interaction forces between the particles. These generate stresses in the particle assembly and give rise to its apparent viscosity.

4. Interactions between the turbulent fluctuations of gas velocity and the mean motion of the gas, which generate the well-known Reynolds stresses.

In view of our incomplete understanding of the structure of turbulence, even in the flow of a single fluid phase through a pipe, it is clear that a treatment including all the above effects is unlikely to be practicable without many arbitrary assumptions. In certain circumstances, however, the first and third effects, which do not involve the gas-phase turbulence directly, can be treated more completely, and the question then arises to what extent these alone are capable of accounting, at least qualitatively, for the various phenomena observed in gas-particle flows.

To formulate a model, even of this restricted type, it is necessary to treat the mutual interactions of the particles. If these are small and light they interact via the motion of the interstitial gas, since this gas acts as a "buffer" which prevents direct contacts between the solid surfaces. For larger and heavier particles, however, the momentum of the moving particles is sufficient to carry them easily through the intervening gas film, and interactions occur by direct collision. Of the two, the second situation is much easier to model, and a theoretical treatment will be limited initially to this case. For the transport of typical mineral particles of 150 μm dia. or larger, it is likely that interaction by direct collision dominates.

The physical mechanisms behind a model of the sort just

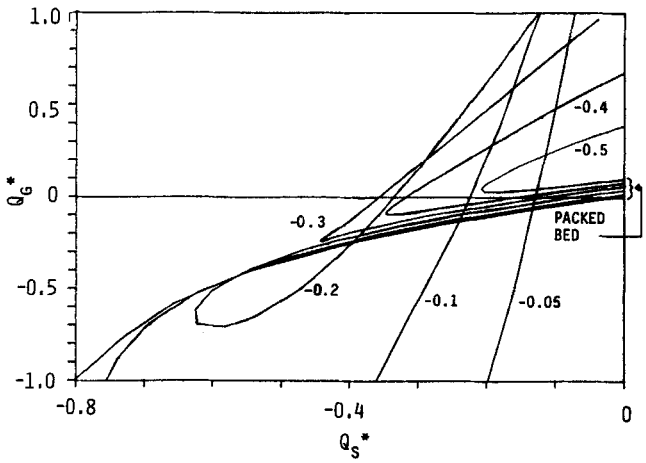

Figure 2. Second and third quadrants of Figure 1.

described can now be summarized. The interaction of the particles and the gas is restricted to a mutual drag force, whose value depends on the concentration of the particles and the difference between the local average values of the velocities of the gas and particle phases. Since the gas does not slip freely at the wall of the pipe there is a gas velocity profile in fully-developed flow, with the maximum velocity on the axis of the pipe, and a corresponding profile of particle velocity is induced by the drag forces exerted by the gas on the particles. As a result of this shearing motion the particles collide with each other, generating a random component of particle motion. The kinetic energy of this random motion is analogous to that of the thermal motion of molecules in a gas and, correspondingly, it can be characterized by a "particle temperature" proportional to the mean square of the random component of the velocity. The particle velocity fluctuations then generate an effective pressure in the particle phase, together with an effective viscosity which resists shearing of the particle assembly. Both the effective pressure and the effective viscosity depend strongly on the particle temperature, as just defined; thus, this must be found by solution of a separate differential equation representing a balance for the so-called pseudothermal energy, that is, the energy of random motion of the particles. Pseudothermal energy is generated by the working of the effective shear stresses in the particle phase, dissipated by the inelasticity of collisions between particles and conducted from place to place as a result of gradients in the particle temperature. Attention will be limited here to a fully-developed flow field, which is generated by simultaneously solving three coupled, ordinary differential equations, representing force balances for the gas and particle phases, and a conservation equation for the pseudothermal energy of the random component of particle motion. The usual conditions of symmetry exist at the axis of the pipe; boundary conditions for the gas velocity, particle velocity, and pseudothermal energy flux must be specified at the pipe wall. In practice, the developing flow that accompanies acceleration of the particles is of considerable importance, and indeed the compressibility of the suspending gas ensures that truly-developed flow is seldom found. Nevertheless, by restricting attention to pipe lengths over which the fractional change in absolute pressure is small, compressibility can be neglected and fully-developed flow is an acceptable approximation.

The mechanical effects of the random component of the gas velocity, whether induced by the particle motion or representing turbulence in response to the overall shearing of the gas phase, are completely neglected. This is clearly improper; for example, we know that motion of the gas in the absence of particles will be incorrectly described for high flow rates, but the object of the present work is simply to determine whether collective effects due to interactions between particles are *alone* capable of accounting qualitatively for the rather complex behavior observed in these systems.

In this paper, we complete an account of a model of the type we sketched recently (1987) for the case of gas-particle flow in vertical tubes.

Equations of Motion

A model of the type outlined above has been constructed and applied to the case of gas-particle flow in a vertical pipe of circular section (Sinclair and Jackson, 1987; Sinclair, 1989). The treatment is limited to situations in which the particles interact

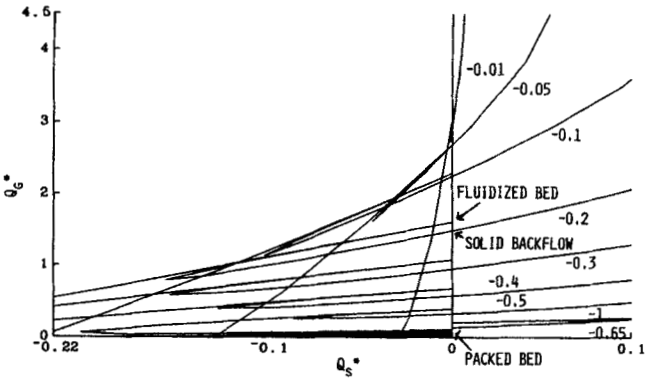

Figure 3. Second quadrant and crossback regions of Figure 1.

with each other only by brief contacts, which can be regarded as collisions. At high concentrations, on the other hand, they will move as a "granular material," with stress generated by normal reactions and frictional forces at points of sustained, sliding and rolling contact. These situations are excluded, though in certain circumstances they are important, even in verticle pipes, and means are available (Johnson and Jackson, 1987) to incorporate their effects.

The equations of motion in cylindrical coordinates, for fully-developed flow, take the following form

$$\mu_{eg}(\nu)\left(\frac{\partial^2 u}{\partial r^2}+\frac{1}{r}\frac{\partial u}{\partial r}\right)-\beta(\nu)(u-v)-\frac{\partial p}{\partial z}=0 \qquad (1)$$

representing an axial force balance for the gas phase,

$$-\frac{\partial \sigma_{rz}}{\partial r}-\frac{\sigma_{rz}}{r}+\beta(\nu)(u-v)-\rho_p \nu g=0 \qquad (2)$$

representing an axial force balance for the particle phase,

$$\frac{\partial \sigma_{rr}}{\partial r}+\frac{\sigma_{rr}}{r}-\frac{\sigma_{\theta\theta}}{r}=0 \qquad (3)$$

representing a radial force balance for the particle phase, and

$$\frac{\partial q_{PT}}{\partial r}+\frac{q_{PT}}{r}+\sigma_{rz}\frac{\partial v}{\partial r}+\gamma=0 \qquad (4)$$

representing a balance for the pseudothermal energy of fluctuating particle velocities.

Here

- u, v = local average axial velocities of gas and particles
- p = pressure of the gas
- σ_{ij} = components of the stress tensor associated with the particle assembly, defined in the compressive sense
- ν = volume fraction of space occupied by the particles
- ρ_p = density of the solid material from which the particles are formed
- g = gravitational acceleration
- μ_{eg} = effective viscosity for the gas phase allowing for the loading with particles
- q_{PT} = radial component of the pseudothermal energy flux
- γ = dissipation rate of pseudothermal energy per unit total volume due to inelastic collisions between the particles.

$\beta(\nu)(u - v)$ = drag force per unit total volume exerted between the phases

A form is assumed for $\beta(\nu)$ based on the Richardson-Zaki (1954) equation

$$\beta(\nu) = \frac{\rho_p \nu g}{v_t(1 - \nu)^n} \tag{5}$$

where v_t is the terminal velocity of fall of an isolated particle under gravity, and the exponent n depends on the Reynolds number under these conditions.

The first term in Eq. 1 represents viscous stresses in the gas phase, the second is the drag force exerted between gas and particles, and third is the force due to the gas pressure gradient. The first two terms in Eq. 2 represent the effect of stress gradients in the particle phase, the third is the reaction of the drag force on the particles, and the last is the gravitational force (this was omitted from the gas-phase force balance because of the low density of the gas). Equation 3 simply equates to zero the radial component of the force due to stress gradients in the particle phase. Derivations of the pseudothermal energy balance Eq. 4 are given by a number of authors, for example, Johnson and Jackson (1987). Physically, the first two terms represent the effect of fluxes of pseudothermal energy, the third accounts for the generation of energy of random motion as a result of shearing the particle phase, and the last gives its rate of dissipation in collisions which are, in general, assumed to be inelastic.

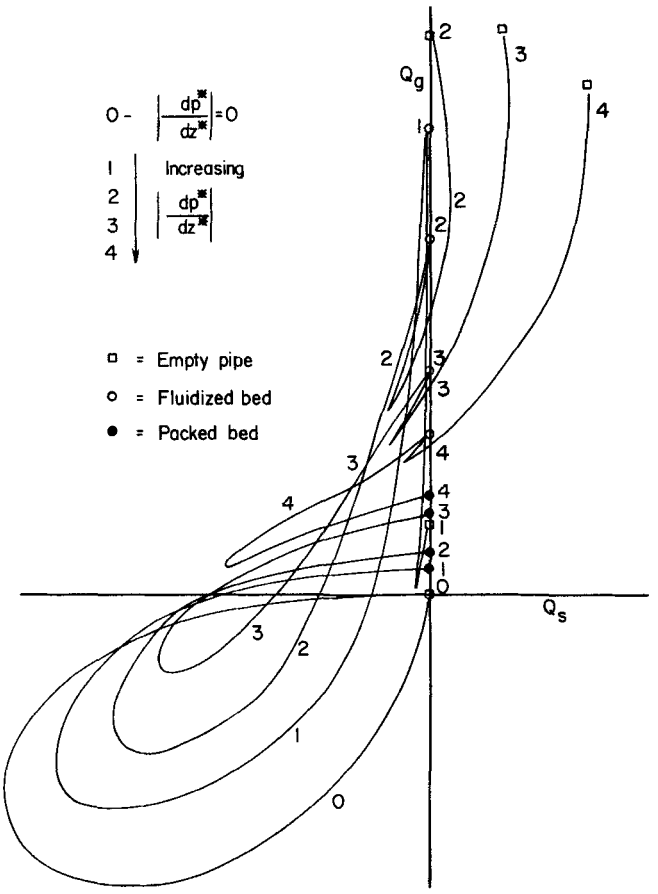

Figure 4. (Q_s^*, Q_g^*) plane illustrating geometric forms of dp^*/dz^* contours.

To close these equations, constitutive relations are needed for the particle phase stress, the pseudothermal energy flux, the dissipation rate, and the gas-phase effective viscosity. The first three of these are chosen to match those used by Johnson and Jackson (1987), which in turn were adopted from earlier work of Lun et al. (1984) and they take the following form

$$\underline{\underline{\sigma}} = [\rho_p \nu T(1 + 4\eta\nu g_o) - \eta\mu_b \nabla \cdot \underline{v}]\underline{\underline{I}} - \left\{\frac{2\mu_i}{g_o}\left(1 + \frac{8}{5}\eta\nu g_o\right)\left[1 + \frac{8}{5}\eta(3\eta - 2)\nu g_o\right] + \frac{6}{5}\mu_b\eta\right\}\underline{\underline{S}} \tag{6}$$

$$q_{PT} = -\frac{\lambda_i}{g_o}\left\{\left(1 + \frac{12}{5}\eta\nu g_o\right)\left[1 + \frac{12}{5}\eta^2(4\eta - 3)\nu g_o\right] + \frac{64}{25\pi}(41 - 33\eta)(\eta\nu g_o)^2\right\}\nabla T - \frac{\lambda_i}{g_o}\left(1 + \frac{12}{5}\eta\nu g_o\right)\frac{12}{5}\eta(2\eta - 1)(\eta - 1)\frac{d}{d\nu}(\nu^2 g_o)\frac{T}{\nu}\nabla\nu \tag{7}$$

$$\gamma = \frac{48}{\pi^{1/2}}\eta(1 - \eta)\frac{\rho_p \nu^2}{d} g_o T^{3/2} \tag{8}$$

The effective viscosity for the gas phase is taken to be

$$\mu_{eg}(\nu) = \mu_g(1 + 2.5\nu + 7.6\nu^2)(1 - \nu/\nu_o)$$

which vanishes when the particles are close-packed with volume fraction ν_o. This means that shearing motion of the gas phase generates no corresponding stress transmitted through this phase, when the particles are at close packing. Although not strictly correct, this is a good approximation because of the dominant effect of drag forces, not only at close packing but down to substantially lower volume fractions (Kim and Russel, 1985), and it helps the numerical work that follows.

In the above relations, $\underline{\underline{S}}$ is the deviatoric part of the rate of deformation tensor for the particle phase

$$\underline{\underline{S}} = \tfrac{1}{2}(\nabla\underline{\underline{v}} + \nabla^T\underline{\underline{v}}) - \tfrac{1}{3}\nabla \cdot \underline{v}\,\underline{\underline{I}}$$

T is the "particle temperature," related to the pseudothermal mean kinetic energy of random motion by $3T/2 = c^2/2$, where c^2 is the mean square velocity fluctuation, while the remaining symbols not previously defined have the following meanings

$$\mu = \frac{5m(T/\pi)^{1/2}}{16d^2} \quad \mu_b = \frac{256\mu\nu^2 g_o}{5\pi} \quad \lambda = \frac{75m(T/\pi)^{1/2}}{64d^2}$$

$$\mu_i = \frac{\mu}{\eta(2 - \eta)} \quad \lambda_i = \frac{8\lambda}{\eta(41 - 33\eta)}$$

$$\eta = \frac{1}{2}(1 + e) \quad g_o = \frac{1}{1 - (\nu/\nu_o)^{1/3}}$$

where μ_i, $\eta\mu_b$, and λ_i represent the shear viscosity, the bulk viscosity, and the pseudothermal conductivity for slightly inelastic particles at the limit of low concentration. There is some doubt about the second group of terms on the righthand side of Eq. 7, which represents a contribution to the flux of pseudothermal energy proportional to the gradient of the particle concentration. Its contribution, however, is small and does not affect the

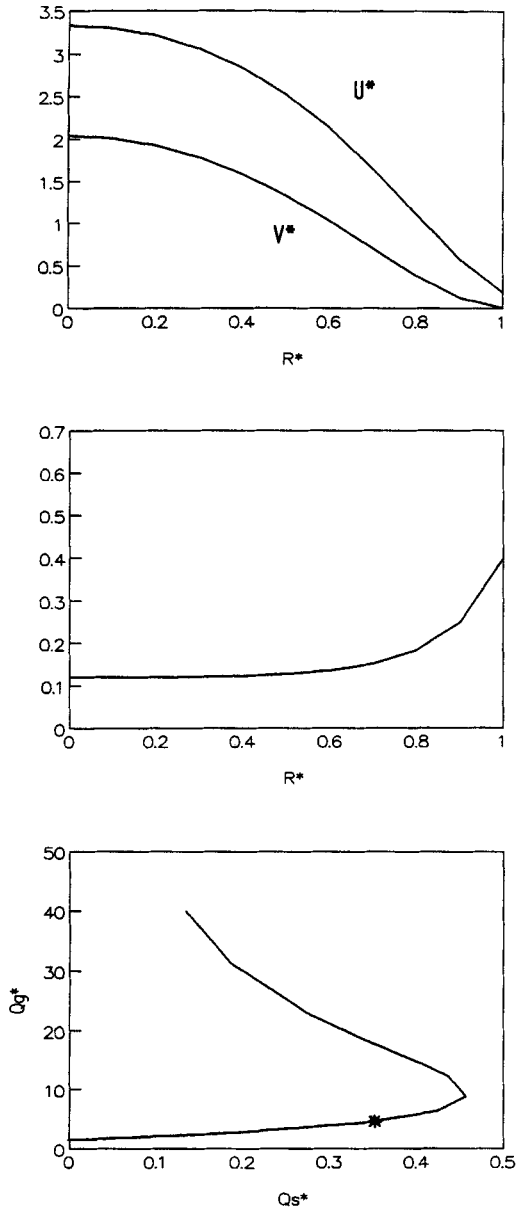

Figure 5. Velocity and particle concentration profiles for $dp^*/dz^* = -0.2$, $Q_s^* = 0.34$, and $Q_g^* = 4.4$.
Mean solids volume fraction is 0.18.

qualitative conclusions, so it has been retained for consistency with earlier work (Lun et al., 1984; Johnson and Jackson, 1987).

Boundary Conditions

To complete the formulation of the problem of fully-developed flow, boundary conditions are needed for the particle velocity and the gas velocity, both at the axis and the wall; conditions must also be imposed on the flux of pseudothermal energy. These will be considered in turn.

A boundary condition for the particle velocity at a solid wall is found by equating the limit of the shear stress in the particle phase, on approaching the wall, to the transfer rate of momentum to the wall by particles that collide with it. An argument of this kind was presented by Hui et al. (1984) using an empirical characterization of the wall in terms of a specularity coefficient, and a more explicit condition for surface roughness of a particular geometric form has been derived by Jenkins and Richman (1986). Here we sketch the argument of Hui et al. and adopt their condition.

The rate of transfer of axial momentum to the wall by particle collisions is the product of three factors, the average collision frequency of each adjacent particle with the wall, given by

$$\frac{(3T)^{1/2}}{d\,[(\nu_o/\nu)^{1/3} - 1]}$$

the average momentum transferred per collision, given by $\phi'\rho_p(\pi d^3/6)v$, and the average number of particles adjacent to

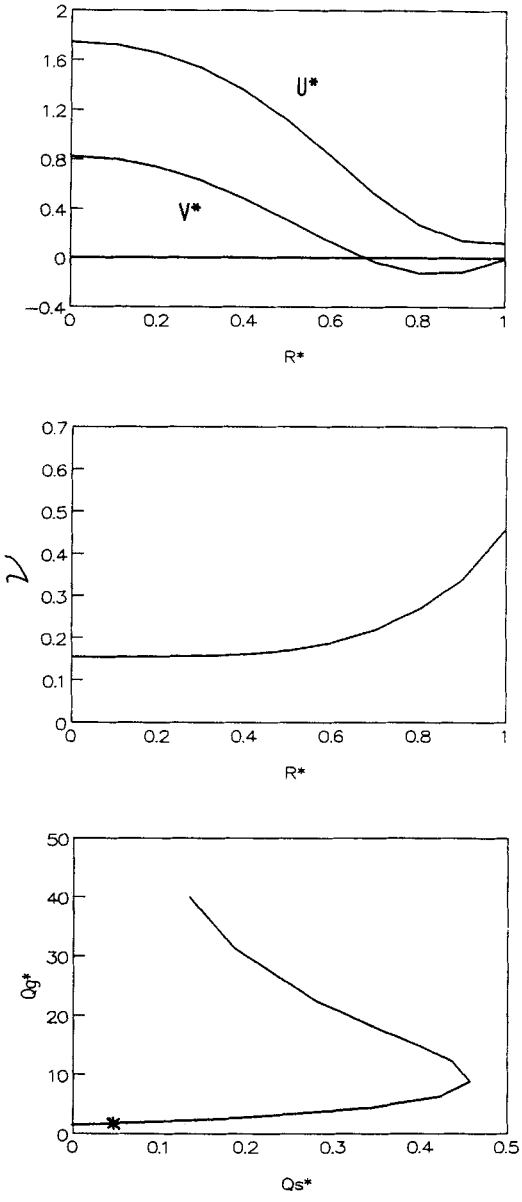

Figure 6. Velocity and particle concentration profiles for $dp^*/dz^* = -0.2$, $Q_s^* = 0.04$, and $Q_g^* = 1.7$.
Mean solids volume fraction is 0.25.

unit area of the surface, given by $1/d^2(\nu_o/\nu)^{2/3}$. Equating this product to the stress then gives

$$\sigma_{rz} = \frac{\phi'\sqrt{3}\ \pi\rho_p\nu\ T^{1/2}\ v}{6\nu_o[1 - (\nu/\nu_o)^{1/3}]} \tag{9}$$

where d is the particle diameter, while ϕ' is a specularity factor, whose value ranges from zero, when collisions between particles and the wall are specular, to unity when incident particles are scattered diffusely.

A boundary condition for the pseudothermal energy flux at the wall is obtained from an energy balance on a thin region adjacent to the solid surface. Details are given by Johnson and Jackson (1987) and by Sinclair (1989), and the result has the form

$$q_{PT} = \gamma_w - v\,\sigma_{rz} \tag{10}$$

Here the lefthand side represents the flux of pseudothermal energy to the wall, the first term on the righthand side is the rate of dissipation of this energy, per unit area, due to the inelasticity of collisions between particles and the wall, and the last term represents generation of pseudothermal energy by slip. Clearly, the wall can serve either as a source or a sink of pseudothermal energy, depending on the relative sizes of the terms on the righthand side. The dissipation term is the product of the average collision frequency of a particle with the wall, the average number of particles adjacent to unit area of the wall, and the average loss of kinetic energy per collision. The first two of these have been given above, and the third is easily seen to be $1/4\pi\rho_p d^3 T(1 - e_w^2)$, where e_w is the coefficient of restitution for particle-wall collisions, so

$$\gamma_w = \frac{\sqrt{3}\ \pi\nu\ \rho_p T^{3/2}\ (1 - e_w^2)}{4\nu_o[1 - (\nu/\nu_o)^{1/3}]}$$

At the axis of the pipe symmetry clearly demands that

$$\frac{\partial v}{\partial r} = \frac{\partial T}{\partial r} = 0 \tag{11}$$

and these complete the set of boundary conditions for the particle velocity and temperature.

An appropriate boundary condition for the gas velocity at the wall is much more difficult to construct. Clearly, the point velocity of the gas will vanish here, but the velocity u appearing in the equations of motion is not this, but some suitable average. Since the point velocity vanishes at the wall in every realization of the system, an ensemble average gas velocity will also vanish there. On the other hand, a local average, generated by spatial averaging over a region large compared with the particle diameter, will not. The ensemble average velocity might be expected to reflect small-scale variations in the statistical properties of the suspension near the wall, but for our purpose we would prefer to avoid dealing with these explicitly, subsuming their effects in some form of effective boundary condition. In doing this, we have a certain amount of guidance from limiting cases; for example, in the limit as $\nu \to 0$, we should recover the Poiseuille solution for flow in an empty tube, so the boundary condition should degenerate into the no-slip condition at this limit. When $\nu \to \nu_o$, on the other hand, we have a packed bed, for which the profile of the local average velocity is known to be essentially flat, so the gas is not "conscious" of the presence of the wall (Kim and Russel, 1985).

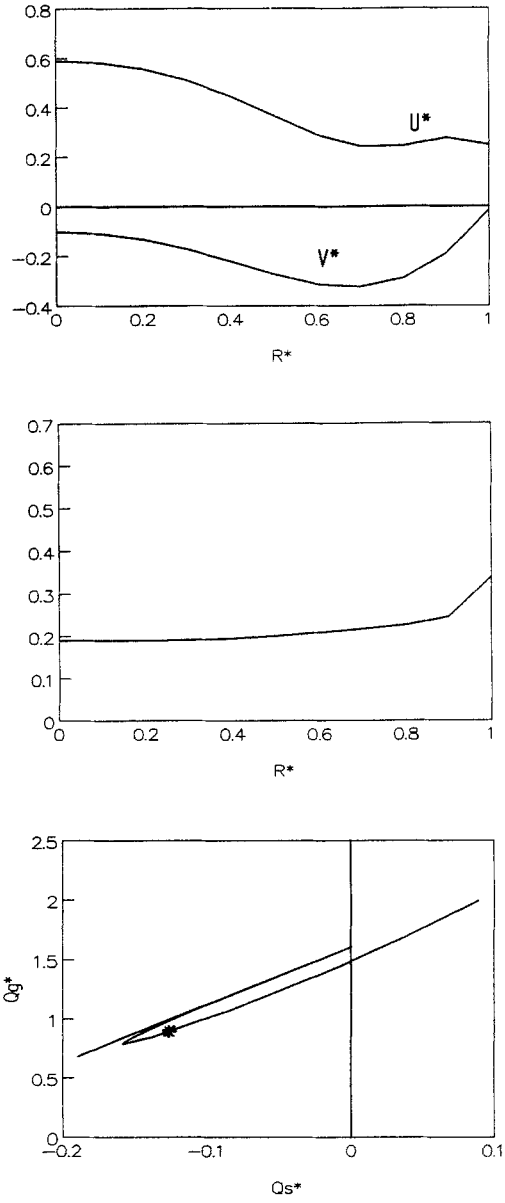

Figure 7. Velocity and particle concentration profiles for $dp^*/dz^* = -0.2$, $Q_s^* = -0.16$, and $Q_g^* = 0.83$.
Mean solids volume fraction is 0.22.

In addition to these limiting cases, it is important to account for the existence of fluidized beds. An ideal fluidized bed is a uniform assembly of particles, of infinite lateral extent, supported at rest by the upward drag force exerted by the gas, which just balances the downward force due to gravity. Such an assembly can exist, in principle, at any value of the particle concentration, provided this and the gas velocity are properly matched so that the forces balance. An infinite bed may be stable or unstable, and there is now quite an extensive literature on the question of stability. What is rather surprising is that beds of this sort are also observed to exist in the presence of lateral bounding walls, though one might expect the drag force on a

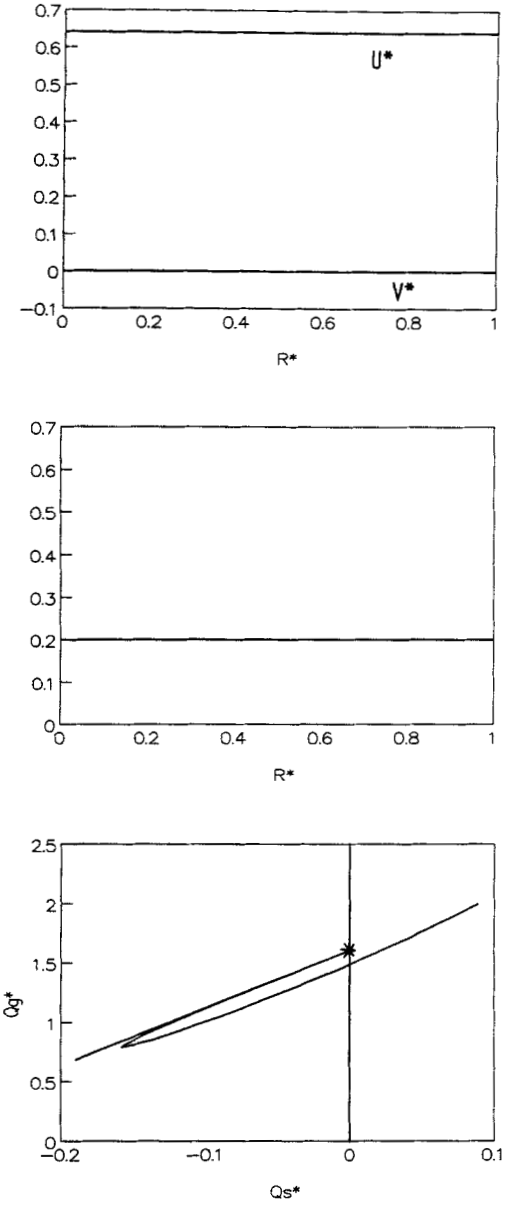

Figure 8. Velocity and particle concentration profiles for $dp^*/dz^* = -0.2$, $Q_s^* = 0$, and $Q_g^* = 1.61$.
Mean solids volume fraction is 0.20.

particle adjacent to such a wall to differ appreciably from the corresponding force on a particle in the body of the bed. Nevertheless, in cases where stable fluidized beds can be formed in tubes of finite diameter, there is no evidence of circulatory motion of those particles in contact with the wall. In constructing a boundary condition for the gas velocity, it is, therefore, important not to choose a form which precludes the possibility of fluidized beds with $\nu < \nu_o$.

With these remarks in mind, our choice of boundary condition is as follows:

$$\beta(\nu)(u - v)\delta(\nu) + \frac{\partial p}{\partial z}\delta(\nu) + \mu_{eg}(\nu)\frac{\partial u}{\partial r} + \frac{\mu_{eg}(\nu)f(T)u}{\delta(\nu)/2} = 0 \quad (12)$$

which has the form of a force balance on the fluid in a layer of thickness $\delta(\nu)$ adjacent to the wall. The first term represents the drag force, the second the force due to the axial gradient of pressure, and the third the shear stress on the surface of the layer remote from the wall. The last term is then a simple estimate of the shear stress at the wall. The purpose of the factor $f(T)$, which is chosen to vanish in the limit $T \to 0$, will be explained below. The layer thickness is assumed to be given by $\delta(\nu) = \delta_o\nu/\nu_o$, where δ_o is the diameter of the averaging region used in defining the local average gas velocity. Then when $\nu \to 0$, the above reduces to the no-slip condition and the Poiseuille solution for gas flow is recovered. At the opposite limit, $\nu \to \nu_o$, the effective viscosity μ_{eg} tends to zero, according to the formula given in the previous section, so the boundary condition reduces to

$$\beta(\nu)(u - v) + \frac{\partial p}{\partial z} = 0 \quad (13)$$

which is just the same force balance as would hold in a bed of infinite extent.

For a solution representing a fluidized bed with concentration ν, other than ν_o, Eq. 13 must be satisfied everywhere, including points adjacent to the wall and u must be independent of r. Thus, for such a solution, the first three terms in Eq. 12 vanish, and the boundary condition can be satisfied only if the last term vanishes also. This is assured by the presence of the factor $f(T)$, since T vanishes for a particle assembly in which $v = 0$ everywhere. The introduction of this factor is, therefore, a device to make the boundary condition consistent with the existence of fluidized beds. Clearly, it is far from a satisfactory way of handling this problem, and the important question of the proper formulation of a boundary condition for the gas phase remains open. For the present, we have chosen a simple dimensionless form for $f(T)$, namely T/v_t^2.

The set of boundary conditions is completed by the requirement that

$$\frac{\partial u}{\partial r} = 0 \quad (14)$$

at the pipe axis.

Limit of Low Particle Concentration

In formulating the gas-phase boundary condition, care was taken to ensure that it approached the no-slip condition at the limit of low particle concentration. It is also necessary, however, to reconsider certain aspects of the equations of motion as this limit is approached. Specifically, the constitutive relation giving the stress tensor in the particle phase is based on the idea that stress is generated by collisions between particles, while particle-wall collisions are taken care of by the boundary condition (Eq. 9). This corresponds closely with the usual treatment of a molecular fluid flow; but, in this case, the picture is well known to break down at very low pressures, where the mean free path length becomes comparable with the pipe diameter. In this Knudsen streaming regime, the motion of the gas is opposed almost entirely by momentum loss in collisions between molecules and the pipe wall, without any intermediate stages of transfer through particle-particle collisions. Though this limiting case can be treated easily, there is no complete and satisfactory theory of the transition region, in which the free path length

is comparable with the pipe diameter. The situation is analogous in the case of the suspension of macroscopic particles. Indeed, in this case, it can be shown (Lun et al., 1984) that, at a given shear rate, the stresses in an infinite shearing assembly of particles tend to infinity as the particle concentration tends to zero. When the assembly is contained within a pipe of fixed diameter, however, this is precluded by the increasingly dominant role of particle-wall collisions as the concentration becomes small.

In the present work, we must address this situation, as we wish to explore the behavior of the moving suspension over the whole range of concentrations. From kinetic theory, the shear viscosity and thermal conductivity for an infinite body of the particle phase are given by

$$\mu = \left(\frac{75\pi}{384}\right)^{1/2} 1\,\nu\,\rho_p\sqrt{T} \qquad \lambda = \frac{75\sqrt{2\pi}}{64} 1\,\nu\,\rho_p\sqrt{T} \quad (15)$$

while the mean free path 1 is related to the concentration ν by $1 = d/6\nu\sqrt{2}$. Using this to eliminate 1 from Eq. 15 gives the expressions for μ and λ presented earlier in connection with the stress constitutive relation for the particles. The above expression for 1 is retained here, so long as it is smaller than the pipe radius a, but when $d/6\nu\sqrt{2} > a$, we set $1 = a$ in Eqs. 15, thus limiting the growth of the mean free path at a value equal to the pipe radius. This rather crude device for effecting a transition to "Knudsen" flow for the particles has the disadvantage that the effective viscosities have discontinuities of slope, when regarded as functions of ν, and this could pose numerical problems. To avoid this, viscosities are further modified by replacing the linear functions of ν, generated by the above procedure for small values of ν, by cubic polynomials which match these lines when

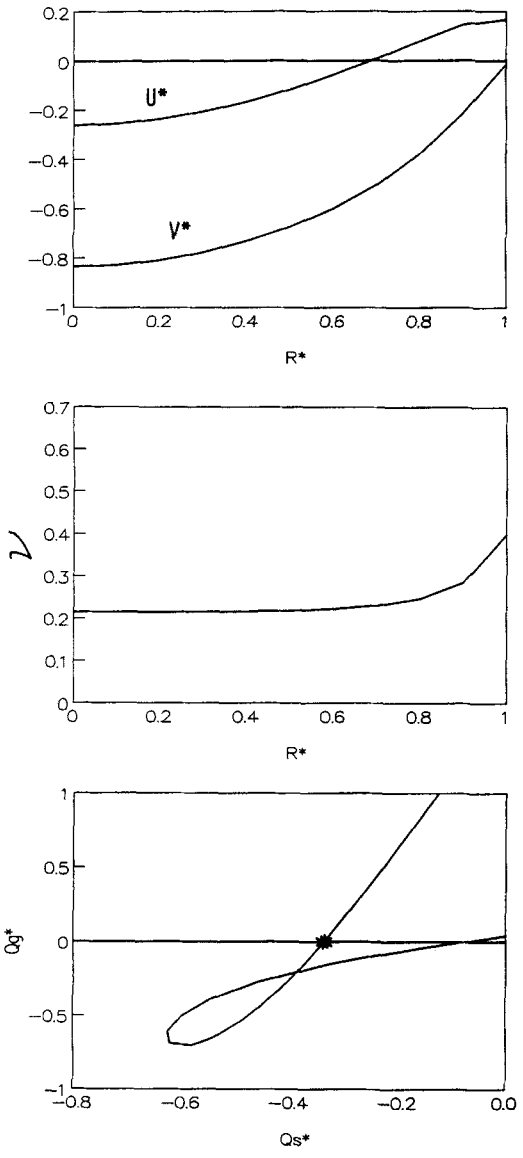

Figure 9. Velocity and particle concentration profiles for $dp^*/dz^* = -0.2$, $Q_s^* = -0.34$, and $Q_g^* = -0.022$.
Mean solids volume fraction is 0.25.

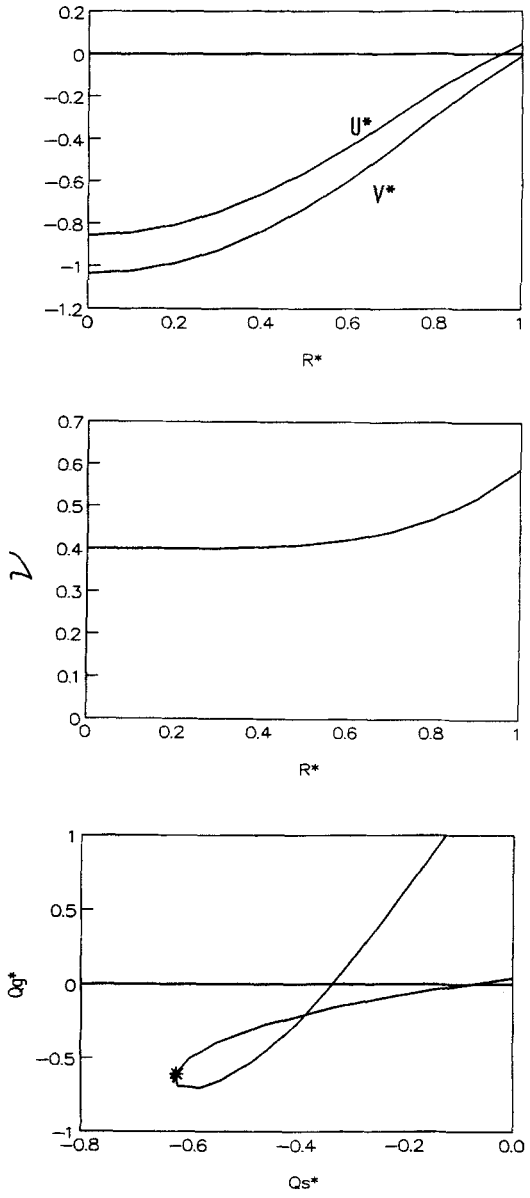

Figure 10. Velocity and particle concentration profiles for $dp^*/dz^* = -0.2$, $Q_s^* = -0.62$, and $Q_g^* = -0.61$.
Mean solids volume fraction is 0.46.

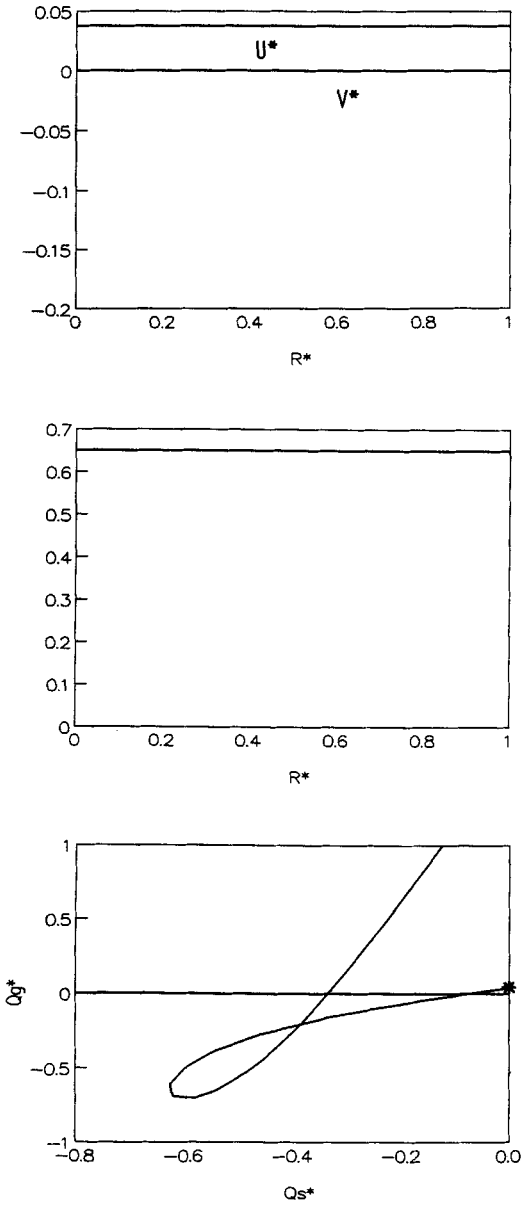

Figure 11. Velocity and particle concentration profiles for $dp^*/dz^* = -0.2$, $Q_s^* = 0$, and $Q_g^* = 0.04$
Mean solids volume fraction is 0.65.

$\nu \rightarrow 0$, but join smoothly to the concentration-independent viscosities at higher concentrations.

With these modifications of the constitutive relations, particle-phase stresses tend to zero on approaching zero particle concentration, and the Poiseuille solution for the gas flow is approached in this limit.

Solution for Fully-Developed Pipe Flow

With the constitutive relations given above, the equations of motion can be written in the following dimensionless form

$$\frac{Re}{Fr}\left[-\frac{\nu(u^*-v^*)}{(1-\nu)^2}-\frac{\partial p^*}{\partial z^*}\right]+\frac{\mu_{eg}^*(\nu)}{r^*}\frac{\partial}{\partial r^*}\left(r^*\frac{\partial u^*}{\partial r^*}\right)=0 \quad (16)$$

$$\frac{\nu}{Fr}\left[\frac{u^*-v^*}{(1-\nu)^2}-1\right]+\frac{d^*}{r^*}\frac{\partial}{\partial r^*}\left[\mu^*(\nu)\sqrt{T^*}f_1(\nu)r^*\frac{\partial v^*}{\partial r^*}\right]=0 \quad (17)$$

$$\frac{1}{r^*}\frac{\partial}{\partial r^*}\left[\lambda^*(\nu)\sqrt{T^*}\left\{f_3(\nu)r^*\frac{\partial T^*}{\partial r^*}+T^*f_4(\nu)r^*\frac{\partial \nu}{\partial r^*}\right\}\right]+\mu^*(\nu)\sqrt{T^*}f_1(\nu)\left(\frac{\partial v^*}{\partial r^*}\right)^2-\frac{f_5(\nu)T^{*3/2}}{d^{*2}}=0 \quad (18)$$

representing the axial components of momentum balance for the gas and particle phases, respectively, and the pseudothermal energy balance. The radial component of the particle-phase momentum balance can be integrated immediately to give

$$f_2(\nu)\,T^* = D \quad (19)$$

where D is a dimensionless integration constant. In these equations, dimensionless variables are distinguished by stars from the dimensional forms of the corresponding variables, and they are defined as follows

$$r^*=\frac{r}{a}\quad z^*=\frac{z}{a}\quad T^*=\frac{T}{v_t^2}$$

$$u^*=\frac{u}{v_t}\quad v^*=\frac{v}{v_t}\quad p^*=\frac{p}{\rho_p a g}$$

$$\mu^*(\nu)=\frac{\mu}{\rho_p d\sqrt{T}}\quad \lambda^*(\nu)=\frac{\lambda}{\rho_p d\sqrt{T}}\quad \mu_{eg}^*(\nu)=\frac{\mu_{eg}(\nu)}{\mu_g} \quad (20)$$

The following dimensionless parameters also appear

$$d^*=\frac{d}{a}\quad \delta^*=\frac{\delta}{a}\quad Re=\frac{\rho_p a v_t}{\mu_g}\quad Fr=\frac{v_t^2}{ga} \quad (21)$$

representing a dimensionless particle diameter, a dimensionless averaging region diameter, a Reynolds number base on the pipe radius and the terminal velocity of fall of an isolated particle in the gas, and a Froude number on the same basis. f_1 through f_5 are dimensionless functions of ν defined in Table 1.

The boundary conditions at the wall ($r^* = 1$) for the gas

Table 1. f_1 to f_5 Dimensionless Functions of ν

$$f_1(\nu)=\left(\frac{1-\frac{\nu^{1/3}}{\nu_0^{1/3}}+\frac{8}{5}\eta\nu+\frac{8}{5}\eta(3\eta-2)\nu+64\eta^2(3\eta-2)\nu^2g_0(\nu)}{\eta(2-\eta)}\right)+\frac{768\eta\nu^2g_0(\nu)}{25\pi}$$

$$f_2(\nu)=\nu[1+4\eta\nu g_0(\nu)]$$

$$f_3(\nu)=\frac{8}{\eta(41-33\eta)}\left(1-\frac{\nu^{1/3}}{\nu_0^{1/3}}+\frac{12}{5}\eta\nu+\frac{12}{5}\eta^2(4\eta-3)\nu+\frac{144}{25}\eta^3(4\eta-3)\nu^2g_0(\nu)+\frac{64(41-33\eta)\eta^2\nu^2g_0(\nu)}{25\pi}\right)$$

$$f_4(\nu)=\frac{8}{\eta(41-33\eta)}\left\{\left(\frac{1}{\nu g_0(\nu)}+\frac{12}{5}\eta\right)\cdot\frac{12}{5}\eta(2\eta-1)(\eta-1)\frac{\partial[\nu^2g_0(\nu)]}{\partial\nu}\right\}$$

$$f_5(\nu)=\frac{48}{\sqrt{\pi}\,\eta(1-\eta)\nu^2g_0(\nu)}$$

velocity, the particle phase velocity, and the particle temperature, take the following form in terms of the dimensionless variables

$$\frac{\partial u^*}{\partial r^*} + d^*\delta^* \frac{Re\, f_6(\nu)}{Fr\, f_7(\nu)}\left[\frac{\nu(u^* - v^*)}{(1-\nu)^2} + \frac{\partial p^*}{\partial z^*}\right] + \mu^*_{eg}(\nu)\frac{d^* T^* u^*}{\delta^* f_7(\nu)} = 0 \quad (22)$$

$$\frac{\partial v^*}{\partial r^*} = -\frac{\phi' f_8(\nu)\, v^*}{d^*} \quad (23)$$

$$d^*\frac{\partial T^*}{\partial r^*} = -(1 - e_w^2) f_9(\nu) T^* + \phi' f_{10}(\nu) v^{*2} - d^*\frac{f_4(\nu)}{f_3(\nu)} T^* \frac{\partial \nu}{\partial r^*} \quad (24)$$

where f_6 through f_{10} are dimensionless functions defined in Table 2. At the axis, we have the boundary conditions

$$\frac{\partial u^*}{\partial r^*} = \frac{\partial v^*}{\partial r^*} = \frac{\partial T^*}{\partial r^*} = 0 \quad (25)$$

and these complete the formulation of the problem.

The above problem contains seven dimensionless parameters, namely Re, Fr, d^*, δ^*, e, e_w, and ϕ', so a complete exploration of the parameter space, for ranges of values of the pressure gradient and the flow rates of the two phases, is clearly impracticable. Instead, we concentrate on one particular case, for which the relevant physical properties are listed in Table 3. These correspond to mineral particles of 150 μm diameter flowing in a pipe of 3 cm diameter, in company with air at 800°F (427°C). (This high temperature was originally chosen because of interest in modeling certain catalytic reactors.) Most of the calculations were made for perfectly elastic collisions between particles and inelastic particle-wall collisions, as indicated by the values of e and e_w in Table 2, but the effect of inelastic collisions between particles was also explored in a limited way.

The solutions were generated along contours of constant pressure gradient $\partial p^*/\partial z^*$. Profiles of gas and particle velocities, particle temperature, and particle concentration were calculated for each of a sequence of values of the integration constant D, which appears in Eq. 19, along each pressure gradient contour. Volume flow rates Q_s and Q_g of the two phases were then found and expressed in dimensionless form as $Q_s^* = Q_s/a^2 v_t$ and $Q_g^* = Q_g/a^2 v_t$.

Since Eq. 19 provides an explicit algebraic relation between T^* and ν, it can be used to eliminate one of these, leaving three differential equations in three unknowns to be solved numerically, subject to two-point boundary conditions. To secure convergence over the whole range of parameter values of interest, a method based on orthogonal collocation (Villadsen and Michelsen, 1978) was found most effective, and details of this are given elsewhere by Sinclair (1989). Ten interior collocation points were enough to give solutions which agreed with analytical results for certain simple limiting cases (for example, gas flow in an empty tube) within 0.01%. Iteration was continued until successive values of the variables u^*, v^* and T^* differed by less than 10^{-6}%, *and* the sum of the absolute values of the residuals of the differential equations was less than 10^{-8}. Other numerical techniques were successful over limited ranges of conditions; for example, a finite difference method converged for low values of the particle concentration, and in these cases its predictions agreed with those of the collocation method.

Table 3. Physical Properties of the Case Used

d	Particle diameter	0.00015 m
ρ_p	Particle material density	2,500 kg/m^3
a	Pipe radius	0.015 m
μ_g	Gas viscosity	0.0365 cp
v_t	Particle terminal velocity	1.29 m/s
e	Particle-particle coefficient of restitution	1.0
e_w	Particle-wall coefficient of restitution	0.9
ϕ'	Specularity coefficient	0.5
ν_o	Solids volume fraction for packed bed	0.65

Table 2. f_6 to f_{10} Dimensionless Functions of ν

$$f_6(\nu) = \frac{\nu^2}{2\nu_0^2}$$

$$f_7(\nu) = \frac{\nu}{2\nu_0}$$

$$f_8(\nu) = \frac{\pi}{\mu^*(\nu) f_1(\nu) 2\sqrt{3}\left(\frac{\nu_0}{\nu} - \frac{\nu_0^{2/3}}{\nu^{2/3}}\right)}$$

$$f_9(\nu) = \frac{\sqrt{3}\,\pi}{\lambda^*(\nu) f_3(\nu) 4\left(\frac{\nu_0}{\nu} - \frac{\nu_0^{2/3}}{\nu^{2/3}}\right)}$$

$$f_{10}(\nu) = \frac{\pi}{\lambda^*(\nu) f_3(\nu) 2\sqrt{3}\left(\frac{\nu_0}{\nu} - \frac{\nu_0^{2/3}}{\nu^{2/3}}\right)}$$

Computed Results

An overall picture of the predicted behavior is best presented as a plot of contours of constant dp^*/dz^* in the (Q_s^*, Q_g^*) plane, Figure 1. Points in the first quadrant then represent cocurrent upflow, points in the third quadrant represent cocurrent downflow, and points in the second quadrant represent countercurrent flow, with the particles descending against an upward flow of gas. Each contour is labelled with the corresponding value of the dimensionless pressure gradient, and it should be recalled that a negative value for this corresponds to pressure decrease on moving up the pipe.

Each curve for a negative pressure gradient terminates on the ordinate axis at some positive value of Q_g^*, even though, for the contours plotted, these values lie beyond the range of the graph. Similarly, each curve for a positive pressure gradient terminates at a point on the negative ordinate axis. In both cases, these points correspond to gas flowing through the pipe in the absence of particles, which we will refer to as empty pipe flow. For a negative value of the pressure gradient, on moving down a given contour the value of Q_s^* first increases, then passes through a maximum and decreases, so that the contour eventually crosses the positive ordinate axis into the second quadrant. At least some of the curves then appear to cross through the second

quadrant and form loops in the third quadrant, but the details of this behavior cannot be seen clearly on the scale of Figure 1.

Figure 2, which is an enlargement of those parts of the second and third quadrants near the origin, reveals some of these details. For values of dp^*/dz^* between -0.2 and -0.05, the pressure gradient contours traverse the second quadrant with positive slope, form loops in the third quadrant whose sizes increase as $|dp^*/dz^*|$ decreases, and then recross the Q_s^* axis and terminate at points on the ordinate axis which, as we shall see, represent the limiting case of gas flow through a stationary packed bed with volume fraction ν_o. When $dp^*/dz^* < -0.3$, on the other hand, the contours turn without forming loops and again terminate at points representing stationary packed beds where they meet the ordinate axis. The part of the second quadrant traversed by the contours is bounded, and its boundary is the envelope of the contours for values of dp^*/dz^* between zero and some value $(dp^*/dz^*)_1$, which is close to -0.3. For values of dp^*/dz^* algebraically smaller than this the pressure gradient contours do not intersect each other, but lie entirely within the above envelope. Clearly the envelope represents flooding conditions in countercurrent flow.

Perhaps the most remarkable behavior is seen in a diagram (Figure 3) scaled to show details of the contours as they traverse the second quadrant. Each contour enters the second quadrant from the first quadrant at a point representing zero net flow rate of particles. After moving down some distance, however, it reverses direction and returns to the ordinate axis at a point not far above that at which it crossed from the first quadrant. Thus, there is a second point with zero net particle flow, and here the curve once again reverses direction and moves down through the second quadrant, eventually returning to the ordinate axis in the manner described above, with or without the formation of a loop depending on the value of dp^*/dz^*. The region of multiplicity generated by the two reversals of direction in the second quadrant has been named the "crossback region" by Sinclair (1989). Its length is seen to be greatest for a value of dp^*/dz^* near -0.2; its physical significance will be discussed below.

Because of the disparity of scales of the various interesting geometric features of the contour map, which has made it necessary to present them on separate diagrams, it is quite difficult to grasp the overall picutre. In Figure 4, we have, therefore, sketched contours with each of the different characteristic geometric forms in their correct relation to each other, but with gross distortions of scale to permit the whole picture to be shown on a single diagram. Henceforth, in discussing the details of flow patterns, we shall refer to this figure rather than attempting to trace the behavior through the segments of a contour drawn to correct scale in the separate Figures 1 through 3.

To explore the flow patterns, we now present plots of velocity profiles and solids volume fraction at a sequence of points along a single pressure gradient contour. The contour $dp^*/dz^* = -0.2$ is a good choice, since it contains examples of all types of behavior. Figure 5a shows velocity profiles and Figure 5b the concentration profile, at the point on the contour identified in Figure 5c. This is a typical example of cocurrent upflow and there is seen to be strong segregation of the particles toward the pipe wall. The influence of the weight of these particles can be seen in the slight concavity of the velocity profiles near the wall. Figure 6 corresponds to a point in the first quadrant quite near where the contour crosses the ordinate axis into the second quadrant. Once again there is strong segregation, but now gravity overcomes the drag force exerted by the gas to make the particles flow down near the wall, whereas they move up near the axis where the gas velocity is larger. At the point where the contour crosses the ordinate axis, it is now clear that upflow near the axis and downflow near the wall balance exactly to give zero net flow of particles.

On moving along the contour through the crossback region, the cross-sectional distribution of particle concentration flattens progressively, as can be seen by comparing Figure 6 with Figure 7. In the latter, there is a true countercurrent flow, with gas flowing up everywhere and particles flowing down, and the segregation of the particles is less pronounced. This trend continues and Figure 8 shows that the apex of the crossback region, where the contour once again meets the ordinate axis, represents a classical fluidized bed with particles distributed uniformly over the section and at rest supported by the drag forces exerted by the gas flow, which is also uniform.

Following the contour down from this point through the second quadrant, the segregation of the particles towards the wall is

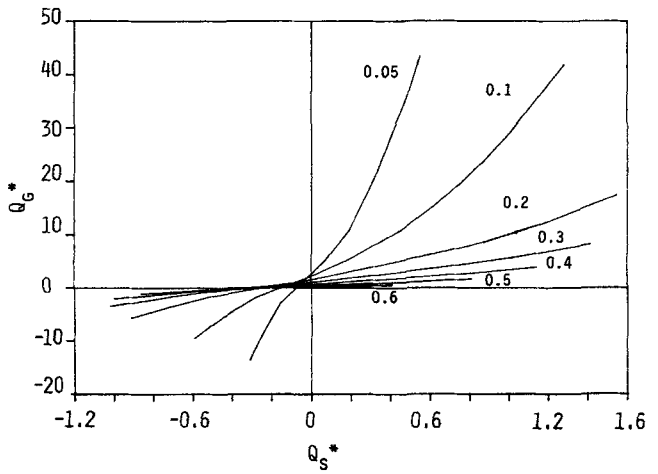

Figure 12. Contours of mean solids volume fraction in the (Q_s^*, Q_g^*) plane.

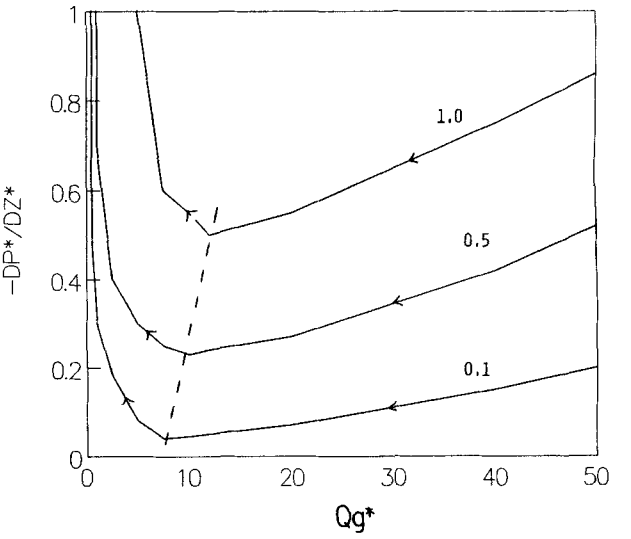

Figure 13. Sections of constant Q_s^* for positive values of this quantity.

progressively reestablished, and the drag forces they exert on the gas begin to distort the gas velocity profile downward in the region near the axis. When the contour crosses into the third quadrant (Figure 9) this effect is pronounced, so that there are balancing gas flows down near the axis and up near the wall. Figures 5 through 9 also show a progressive increase in overall particle concentration on moving along the contour and this continues throughout its length.

Figure 10 shows a typical cocurrent downflow. Since the pressure falls on moving up the pipe, the gas must be dragged down by the particles, so the gas velocity is algebraically larger than the particle velocity. This situation is reversed, of course, on contours of positive pressure gradient. The overall particle concentration is now high, and there is again a marked segregation toward the wall. Along the last part of the contour, as it emerges from the loop in the third quadrant and moves back to the right in the second quadrant, the overall particle concentration increases rapidly, the distribution flattens once more and the particle velocity decreases everywhere, approaching zero as the contour heads to its final meeting with the ordinate axis. Conditions at this terminal point are shown in Figure 11, and they clearly represent a stationary packed bed traversed by a uniform flow of gas.

It is interesting that this contour, and most others with negative pressure gradients, encounter the axis $Q_s^* = 0$ four times, and three of these intersections correspond to situations for which simple analytic solutions of the equations of motion exist. At the first intersection, corresponding to empty pipe flow, it follows from the Poiseuille solution for the gas flow that

$$Q_g^* = -\frac{\pi \rho_p g a^2}{8 \mu_g v_t}\frac{\partial p^*}{\partial z^*} \quad Q_s^* = 0 \tag{26}$$

The third intersection represents a fluidized bed, and here

$$Q_g^* = \pi(1-\nu)^3 \quad Q_s^* = 0 \quad \frac{\partial p^*}{\partial z^*} = -\nu \tag{27}$$

while the last intersection is a stationary packed bed, for which

$$Q_g^* = -\frac{\pi(1-\nu_o)^3}{\nu_o}\frac{\partial p^*}{\partial z^*} \quad Q_s^* = 0 \tag{28}$$

From Eq. 27, it is seen that the point on the ordinate axis with $Q_g^* = \pi$ corresponds to a fluidized bed of infinite dilution, while $Q_g^* = \pi(1-\nu_o)^3$ represents a bed at minimum fluidization. Fluidized beds exist only in this interval, where different points represent beds with varying degrees of expansion. On the other hand, from Eqs. 26 and 28, any point of the ordinate axis can represent empty tube flow or packed bed flow for some value of the pressure gradient. This has a curious consequence for contours corresponding to negative pressure gradients of very small magnitude. For the contour $dp^*/dz^* = -0.2$, explored in detail above, the point on the ordinate axis representing empty tube flow lies above the point representing a fluidized bed. However, from Eqs. 26 and 27, when $dp^*/dz^* \rightarrow 0$ through negative values, Q_g^* increases toward π for the fluidized bed while it decreases toward zero for the empty pipe. Thus, for negative pressure gradients of sufficiently small magnitude, the relative positions of the fluidized bed and empty pipe points are reversed with the former lying above the latter. This is seen in contour 1 in Figure 4.

Of course, this situation is physically unrealistic. When particles are suspended at very low concentration in a gas flowing in a vertical pipe, they do not form a fluidized bed, even though fluidized beds of *infinite* lateral extent can exist, in principle, for arbitrarily small values of the particle concentrations. This situation has arisen because of the factor $f(T)$ introduced into the boundary condition (Eq. 12). The purpose of this was to admit the existence of classical fluidized beds, even in pipes of bounded diameter, and in this respect it has been rather too successful since it ensures their existence at *all* values of the overall particle concentration. The important question of an appropriate boundary condition for the gas at a solid bounding surface therefore remains open.

In general, as indicated above, the cross-sectional average value of the solids volume fraction increases on moving along the contour curves away from the point representing empty tube flow. This can be quantified by plotting contour curves of overall solids volume fraction in the (Q_s^*, Q_g^*) plane, as shown in Figure 12. However, the scale of this diagram hides the rather complicated form taken by the contours in the second quadrant as a result of the crossback regions on the pressure gradient contours.

While the plot of contours of dp^*/dz^* in the plane of solids and gas flow rates, as presented above, gives a compact overview of the system, for the purpose of predicting behavior in physically specified situations it is more convenient to represent the data as sections of this diagram at constant solid flow rate with the pressure gradient and the gas flow rate as coordinates. Figure 13 shows sections of this type for several positive values of the solids flow rate. The form of these is familiar, with each curve passing through a minimum. The locus of these minima was chosen by Zenz and Othmer (1960) as the demarcation between "lean" and "dense" regimes of cocurrent upflow. Whether or not multiple flow regimes are possible for given imposed conditions depends on the nature of these conditions. Thus, if the values of the gas and particle flows are imposed, there is a unique flow regime, while if values for the particle flow and the pressure gradient are imposed, there is either no solution

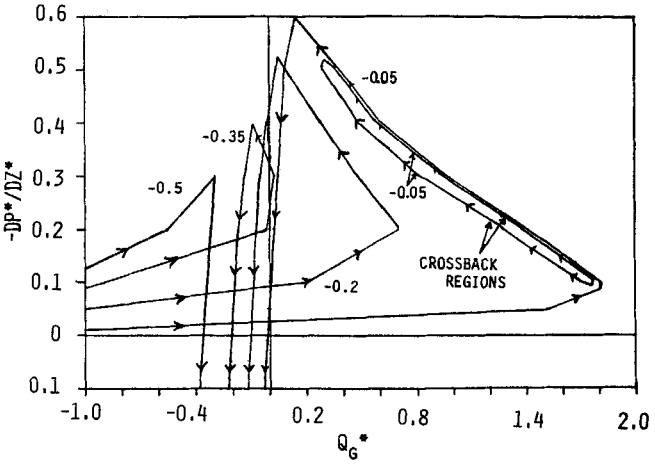

Figure 14. Sections of constant Q_s^* for negative values of this quantity.

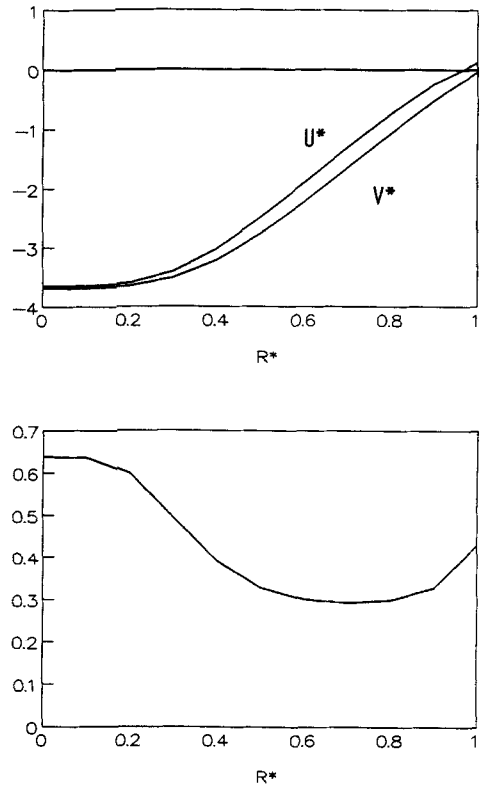

Figure 15. Velocity and particle concentration profiles for $dp^*/dz^* = -0.2$, $Q_s^* = -2.10$, and $Q_g^* = -2.83$.

Inelastic collisions with $e = 0.99$.

in the first quadrant or two solutions with different values of the gas flow. If the gas is driven through the pipe by a compressor, the situation lies between these extremes and the possibility of multiplicity can be determined by superimposing the compressor characteristic on the diagram.

Corresponding sections for some negative values of the particle flow rate are presented in Figure 14 and are seen to be more complex than those in Figure 13. For particle flow rates of small magnitude the section cuts the crossback regions of the pressure gradient contours, and this has the effect of generating a separate loop isolated from the rest of the curve, as seen in the section for $Q_s^* = -0.05$. In addition, the remaining part of this curve intersects itself to form a much larger loop which encloses the small loop generated by the crossback regions, and this large loop remains a feature of all the sections for values of dp^*/dz^* between zero and -0.35. In this very complex situation, there are clearly many possibilities for multiple flow regimes under given imposed conditions and the question of stability of the states lying on various arcs of these sections becomes important.

All the results presented above correspond to a system in which collisions between particles are perfectly elastic, while collisions between particles and the pipe wall are inelastic with $e_w = 0.9$. Calculations were also made for inelastic collisions between particles, and the distribution of the particles over the cross section is then more complicated. Figure 15 shows the radial distribution of particle concentration in a particular cocurrent downflow for a case in which $e = 0.99$ and $e_w = 0.9$. It is seen that the concentration is largest on the axis of the pipe, decreases to a minimum on moving away, and then increases again on approaching the wall. Other forms of concentration distribution are found for different values of the flow rates of the two phases, and a more complete account of these is given by Sinclair (1989).

Conclusions

From the results presented, it appears that collective effects due to interactions between particles are capable of generating the sort of segregation of particles and gas that is observed in practice; taking these effects into account introduces a rich variety of behavior not seen in models which assume a uniform distribution of particle concentration or impose an arbitrary distribution. Some of this new behavior, such as the existence of several different states of zero solid flow rate for a given pressure gradient, clearly corresponds to what is observed in practice. Other features, such as the loops in the third quadrant of the (Q_s^*, Q_g^*) plane, which indicate the possibility of more than one state of cocurrent downflow for given imposed conditions, match reported, but not yet well established behavior. Unfortunately, detailed and comprehensive experimental data for countercurrent flow and both types of cocurrent flow in a given pipe, including profiles of particle concentration and the velocities of both phases, are not available. Quantitative comparisons of the predictions with experiment are not, therefore, possible. However, such comparisons would probably be premature at the present stage, since the model takes no account of obviously important phenomena such as turbulence, whose presence would be expected to have a marked influence on the particle concentration distribution. The value of the results is in their indication of the remarkable qualitative effects that are generated by the interaction forces between particles.

The modeling also reveals the important role of the boundary condition for the gas at the pipe wall, and the inadequacy of our present attempt to formulate such a boundary condition. Of course, the point gas velocity satisfies a no-slip condition at the wall, and it follows that an ensemble average of this velocity will also vanish at the wall. However, the local volume average velocity at the wall depends on the way the averaging region is chosen there, and its value will not vanish. It is tempting to conclude that the equations should be formulated in terms of ensemble averages, but unfortunately these will vary rapidly on the scale of the particle diameter in the neighborhood of the wall. For the purpose of predicting the behavior of the bulk of the suspension, one would like to avoid consideration of these small-scale variations by subsuming their effect in some appropriate "boundary condition," but the form this should take is not yet clear. As noted earlier, the boundary condition used in the present work predicts the existence of classical fluidized beds within the pipe down to arbitrarily small values of the particle concentration, which is not in accord with observations.

Acknowledgment

This work is supported by the National Science Foundation, Particulate and Multiphase Processes Program under grant number CBT-8504201 A03 and by the International Fine Particle Research Institute. The first author also wishes to acknowledge personal support in the form of a National Science Foundation Fellowship.

Notation

a = pipe radius
d = particle diameter
D = integration constant in Eq. 19
e = coefficient of restitution for particle-particle collisions
e_w = coefficient of restitution for particle-wall collisions
f_1–f_{10} = dimensionless functions defined in Tables 1 and 2
Fr = Froude number defined in Eq. 21
g = gravitational acceleration
g_o = radial distribution function
l = mean free path for particle-particle collisions
m = mass of a single particle
n = Richardson-Zaki exponent, Eq. 5
p = gas pressure
q_{PT} = magnitude of pseudothermal energy flux
Q_g = volumetric flow rate of gas
Q_s = volumetric flow rate of particulate solids
r = radial coordinate
Re = Reynolds number defined in Eq. 21
S = deviatoric part of rate of deformation tensor
T = particle temperature
u = magnitude of gas velocity
v = magnitude of particle velocity
v_t = terminal velocity of fall of a single particle in the gas
z = axial coordinate

Greek letters

$\beta(\nu)$ = drag coefficient defined in Eq. 5
γ = rate of dissipation of pseudothermal energy per unit volume by collisions
γ_w = rate of dissipation per unit area of wall by collisions
δ = thickness of averaging region adjacent to wall for gas boundary condition
λ = pseudothermal conductivity of dilute assembly of elastic particles
λ_i = pseudothermal conductivity of dilute assembly of slightly inelastic particles
μ = shear viscosity of dilute assembly of elastic particles
μ_i = shear viscosity of dilute assembly of slightly inelastic particles
μ_b = bulk viscosity of dilute assembly of elastic particles
μ_g = gas viscosity without particles
μ_{eg} = effective gas viscosity in presence of particles
ν = fraction of volume occupied by particles
ν_o = maximum possible value for ν
ρ_p = density of solid material
ϕ' = specularity factor for particle-wall collisions

Literature Cited

Arastoopour, H., and C. Cutchen, "Measurement and Analysis of Particle-Particle Interaction in a Cocurrent flow of Particles in a Dilute Gas-Solids System," *Chem. Eng. Sci.*, **40,** 1135 (1985).

Aarastoopour, H., C. Wang, and S. Weil, "Particle-Particle Interaction force in a Dilute Gas-Solids System," *Chem. Eng. Sci.*, **37,** 1379 (1982).

Bartholomew, R., and R. Casagrande, "Measuring Solids Concentration in Fluidized Systems by Gamma-Ray Absorption," *Ind. Eng. Chem.*, **49,** 428 (1957).

Berker, A., and T. Tulig, "Hydrodynamics of Gas-Solids Flow in a Catalytic Cracker Riser: Implications for Reactor Sensitivity Performance," *Chem. Eng. Sci.*, **41,** 821 (1986).

Chen, Y-M., S. Rangachari, and R. Jackson, "A Theoretical and Experimental Investigation of Flow in a Vertical Standpipe," *I/EC Fund.*, **23,** 354 (1984).

Gidaspow, D., and C. Solbrig, "Transient Two Phase Flow Models in Energy Production," *AIChE Meeting* (1976).

Ginestra, J. C., S. Rangachari, and R. Jackson, "A One-Dimensional Theory of Flow in Vertical Standpipes," *Powder Technol.*, **27,** 69 (1980).

Hinze, J., "Momentum and Mechanical Energy Balance Equations for a Flowing Homogeneous Suspension with Slip Between the Two Phases," *Appl. Sci. Res.*, **11,** 33 (1962).

Hui, K., P. K. Haff, J. Ungar, and R. Jackson, "Boundary Conditions for High Shear Grain Flows," *J. Fluid Mech.*, **145,** 223 (1984).

Jenkins, J., and M. Richman, "Boundary Conditions for Plane Flows of Smooth, Nearly Elastic, Circular Discs," *J. Fluid Mech.*, **171,** 53 (1986).

Johnson, P. C., and R. Jackson, "Frictional-Collisional Constitutive Relations for Granular Materials with Application to Plane Shearing," *J. Fluid Mech.*, **176,** 67 (1987).

Kim, S., and W. B. Russel, "Modelling of Porous Media by Renormalization of the Stokes Equations," *J. Fluid Mech.*, **154,** 269 (1985).

Leung, L. S., and P. Jones, "Coexistence of Fluidized Solids Flow and Packed Flow in Standpipes," *Proc. Int. Fluidization Conf.*, **116,** *Cambridge Univ. Press,* (1978).

Lun, C., S. B. Savage, D. Jeffrey, and N. Chepurniy, "Kinetic Theories for Granular Flow: Inelastic Particles in Couette Flow and Slightly Inelastic Particles in a General Flow Field," *J. Fluid Mech.*, **140,** 223 (1984).

Richardson, J., and W. Zaki, "Sedimentation and Fluidization: Part I," *Trans. Instn. Chem. Engrs.*, **32,** 35 (1954).

Saxton, A., and A. Worley, "Modern Catalytic Cracking Design," *Oil and Gas J.*, **68,** 82 (1970).

Sinclair, J. L., "Vertical Transport of Gas and Solids with Radial Solid Density Variations," *PhD Diss., Princeton Univ.* (1989).

Sinclair, J. L., and R. Jackson, "The Flow of Gas and Solid Particles in Vertical Tubes," *AIChE Meeting, New York* (1987).

Villadsen, J., and M. L. Michelsen, *Solution of Differential Equation Models by Polynomial Approximation,* Prentice-Hall, Englewood Cliffs, NJ (1978).

Weinstein, H., M. Shao, and L. Wasserzug, "Radial Solid Density Variation in a Fast Fluidized Bed," *AIChE Symp. Ser.*, **80,** 117 (1984).

Yerushalmi, J., M. Cankurt, D. Geldart, and B. Liss, "Flow Regimes in Vertical Gas-Solid Contact Systems," *AIChE Symp. Ser.*, **74,** 1 (1978).

Youchou, L., and M. Kwauk, "The Dynamics of Fast Fluidization," *Fluidization,* J. Grace and J. Matsen, eds., Plenum Press, New York (1980).

Zenz, F., and D. Othmer, *Fluidization and Fluid Particle Systems,* Reinhold Publishing Co., New York (1960).

Manuscript received Mar. 28, 1989, and revision received June 14, 1989.